The Dynamic Architecture of *Hox* Gene Clusters

Daan Noordermeer, *et al.*

Science **334**, 222 (2011);
DOI: 10.1126/science.1207194

After the shell containing the red compound was abandoned, it was covered with aeolian dune sand derived from layer CP, as was the case for Tk-S1.

A small quartzite core (Tk2-L1) rested on the shell nacre close to the anterior edge (figs. S24 and S27). The core was used first to grind ferruginous lutites, composed in one case of goethite, calcite, and quartz, and in the other of hematite, calcite, and quartz (figs. S28 and S29 and table S2). Several flakes were then removed from the utilized area, and the object was again used to grind a type FS1 red ferruginous siltstone. A large fragment of ochre (Tk2-P1) composed of ferruginous siltstone FS1 lay 5 cm southwest of the shell (fig. S30). It was knapped to produce small flakes, similar to those in the red compound from Tk1-S1 and Tk2-S1. The piece was also rubbed against a hard stone to produce ochre powder (figs. S31 and S32).

The two *Haliotis* shells derive from the infratidal zone, at that time a few hundred meters from the cave (*16*). Before their use as containers, the respiratory holes of the *Haliotis* were possibly plugged. When recovered, these holes were filled with detritus (fig. S6), but this could have occurred postdepositionally. The ochre and silcrete were sourced from at least several kilometers away (*9*), and the rest of the objects that make up the toolkits were available in the immediate environment.

We infer that manufacturing proceeded as follows: Pieces of ochre (FS1 and FS2) were rubbed on quartzite slabs to produce a fine red powder, and some were knapped with large lithic flakes. The ochre chips resulting from the latter were crushed with quartz, quartzite, and silcrete hammerstones/grinders. Quartzite grinders were used to crush goethite or hematite-rich lutite. Medium-sized mammal bone was crushed, probably with a stone hammer. The red or reddish brown color and cracked, flaky texture of some of the trabecular bone suggest that it was heated before crushing, probably to enhance the extraction of the marrow fat. The hematite powder, charcoal, crushed trabecular bone, stone chips, and quartz grains and a liquid were then introduced into the *Haliotis* shells and gently stirred (figs. S5, S25, and S26). Charcoal is rare in the layer-CP matrix, suggesting that it was a deliberate addition to the mix. The quartz and quartzite chips, produced during the action of crushing the ochre, and the quartz grains may have been incidentally incorporated.

The application or use of the compound is not self-evident. No resins or wax were detected that might indicate it was an adhesive for hafting. Possible uses could include painting a surface in order to decorate or protect it, or to create a design. Ochre residues on the bone Tk1-B1 show that it was possibly used as a stirrer and also to transfer some of the compound out of the shell. At least some of the components of the toolkit were reused, suggesting that production was not a one-time event. An example is the first use of the grinder Tk2-L1 to grind yellow goethite, its subsequent reduction by flaking, and then its reuse to grind red ochre. The ochre FS2 is present only in Tk1, and the stone tools found in close association with each shell may have been exclusive to the processing related to that shell. However, the close proximity of the two toolkits suggests that they were used contemporaneously. Because both toolkits were left in situ, and because there are few other archaeological remains in the CP layer, it seems that the site was used primarily as a workshop and was abandoned shortly after the compounds were made. Aeolian sand then blew into the cave from the outside, encapsulating the toolkits (Fig. 2).

Recent support for a southern African origin for *Homo sapiens* comes from genomic and phenomic diversity studies (*17*, *18*). The recovery of these toolkits at Blombos Cave adds evidence for early technological and behavioral developments associated with *H. sapiens* and documents their deliberate planning, production, and curation of a pigmented compound and the use of containers. *H. sapiens* thus also had an elementary knowledge of chemistry and the ability for long-term planning.

References and Notes

1. E. Hovers, S. Ilani, O. Bar-Yosef, B. Vandermeersch, *Curr. Anthropol.* **44**, 491 (2003).
2. C. S. Henshilwood, F. d'Errico, I. Watts, *J. Hum. Evol.* **57**, 27 (2009).
3. I. Watts, *J. Hum. Evol.* **59**, 392 (2010).
4. F. d'Errico, H. Salomon, C. Vignaud, C. Stringer, *J. Archaeol. Sci.* **37**, 3099 (2010).
5. L. Wadley, T. Hodgskiss, M. Grant, *Proc. Natl. Acad. Sci. U.S.A.* **106**, 9590 (2009).
6. L. Wadley, *J. Archaeol. Sci.* **37**, 2397 (2010).
7. A. Šajnerová-Dušková, J. Fridrich, I. Fridrichová-Sýkorová, in *Non-flint Raw Material Use in Prehistory: Old Prejudices and New Directions,* F. Sternke, L. J. Costa, L. Eigeland, Eds. (Archeopress, Oxford, 2009), pp. 145–151.
8. P. Van Peer *et al.*, *J. Hum. Evol.* **45**, 1 (2003).
9. C. S. Henshilwood *et al.*, *J. Archaeol. Sci.* **28**, 421 (2001).
10. Z. Jacobs, R. G. Roberts, *Evol. Anthropol. Issues News Rev. (Melb.)* **16**, 210 (2007).
11. Z. Jacobs, G. A. T. Duller, A. G. Wintle, C. S. Henshilwood, *J. Hum. Evol.* **51**, 255 (2006).
12. C. Tribolo *et al.*, *Archaeometry* **48**, 341 (2006).
13. H. P. Schwarcz, *Archaeometry* **22**, 3 (1980).
14. D. A. Richards, J. A. Dorale, *Rev. Mineral. Geochem.* **52**, 407 (2003).
15. Information on materials and methods is available on *Science* Online.
16. J. S. Compton, *Quat. Sci. Rev.* **30**, 506 (2011).
17. B. M. Henn *et al.*, *Proc. Natl. Acad. Sci. U.S.A.* **108**, 5154 (2011).
18. Q. D. Atkinson, *Science* **332**, 346 (2011).

Acknowledgments: C.S.H. and F.D. received funding from the European Research Council (ERC) under the European Union's Seventh Framework Programme (FP7/2007-2013)/ ERC grant agreement no. 249587, the PROTEA French–South African research program, and the Groupe de Recherche International STAR of the CNRS. C.S.H. was also funded by a National Research Foundation/ Department of Science and Technology–supported chair at the University of the Witwatersrand, South Africa, and by a joint Norwegian Research Council/ South African National Research Foundation grant; and Z.J. was funded by Australian Research Council Discovery project grant DP1092843. The data described in the paper are presented in the supporting online material. C.S.H. and K.vN. excavated the toolkits; C.S.H., F.D., K.vN., and R.G.-M. wrote the text; Z.J. and S.-E.L. wrote the dating text; and all authors were involved in aspects of the data analysis. All the authors discussed the results and implications and commented on the manuscript at all stages. The authors declare no competing interests.

Supporting Online Material

www.sciencemag.org/cgi/content/full/334/6053/219/DC1
Materials and Methods
SOM Text
Figs. S1 to S45
Tables S1 to S6
References (*19*–*50*)

21 July 2011; accepted 31 August 2011
10.1126/science.1211535

The Dynamic Architecture of *Hox* Gene Clusters

Daan Noordermeer,[1] Marion Leleu,[1] Erik Splinter,[2] Jacques Rougemont,[1,3] Wouter De Laat,[2] Denis Duboule[1,4]*

The spatial and temporal control of *Hox* gene transcription is essential for patterning the vertebrate body axis. Although this process involves changes in histone posttranslational modifications, the existence of particular three-dimensional (3D) architectures remained to be assessed in vivo. Using high-resolution chromatin conformation capture methodology, we examined the spatial configuration of *Hox* clusters in embryonic mouse tissues where different *Hox* genes are active. When the cluster is transcriptionally inactive, *Hox* genes associate into a single 3D structure delimited from flanking regions. Once transcription starts, *Hox* clusters switch to a bimodal 3D organization where newly activated genes progressively cluster into a transcriptionally active compartment. This transition in spatial configurations coincides with the dynamics of chromatin marks, which label the progression of the gene clusters from a negative to a positive transcription status. This spatial compartmentalization may be key to process the colinear activation of these compact gene clusters.

During mammalian development, *Hox* genes are activated sequentially relative to their positions along the four genomic clusters (*HoxA* to *HoxD*). As a result, this process leads to a corresponding distribution of transcripts along the rostral-to-caudal body axis. This process of

colinear activation is essential for the organization of the body plan (*1*, *2*). Accompanying this process, a dynamic transition occurs in the chromatin microenvironment, from a repressive (histone H3K27me3) to a transcription-permissive (histone H3K4me3) state (*3*). Changes in higher-order chromatin organization have been reported to accompany the transcription of developmentally relevant genes (*4*), and the 3D organization of the *HoxA* cluster is changed upon gene activation in mammalian cultured cells (*5*–*7*). Furthermore, the *HoxB* and *HoxD* clusters adopt a decondensed conformation along with gene activation (*8*, *9*) accompanied by modifications of the Polycomb repressive complex 1, as shown in cultured cells (*10*). We analyzed the architectures of these genomic loci in embryonic tissues at different stages of the colinear transcriptional activation and describe a bimodal state, where active and inactive genes are found in distinct three-dimensional (3D) domains and genes progressively lose their interactions with the repressive domain to associate with a transcriptionally active structure.

We used gene expression microarrays to compare *Hox* gene activity in three tissue samples obtained from embryonic day 10.5 (E10.5) mouse embryos: "anterior" dorsal trunk cells (from upper forelimb to upper hindlimb levels), "posterior" dorsal trunk cells (from upper forelimb level to tailbud), and forebrain cells. The latter cells do not express any *Hox* genes and were used as negative control (Fig. 1A, fig. S1, and table S1). We determined which genes were either transcribed or silent in these samples and positioned the dissection limit between the two trunk samples approximately at the level of the *Hoxd10* expression boundary (Fig. 1A, arrowheads; fig. S1 and table S2).

Using these tissue samples, we examined the 3D architecture by high-resolution chromatin conformation capture [Multiplex 4C-seq (*11*, *12*); fig. S2 and table S3] with multiple genes as anchor points ("viewpoints"), taken in all four *Hox* clusters (figs. S3 to S5 and table S4). Although most of the intrachromosomal associations were restricted to the *Hox* clusters themselves (Fig. 1B and fig. S6), a statistical algorithm reliably identified nondynamic long-range interaction landscapes surrounding each locus and extending slightly past the flanking gene deserts (*13*), which may reflect a generic organization of *Hox* clusters and their surroundings in these cells (Fig. 1B, fig. S6, and table S5).

We quantified intracluster 3D organization at highest resolution [figs. S5 and S7 (*11*)], using the *HoxD* cluster in forebrain cells, where all *Hox* genes are inactive. Seven different viewpoints revealed comparable domains of 3D association, spanning from *Evx2* to a few kilobases downstream of *Hoxd1* (Fig. 1C and fig. S7). Likewise, three viewpoints within each of the other *Hox* clusters uncovered association domains covering the entire clusters plus a few kilobases on either side (fig. S8). Therefore, silent *Hox* clusters form 3D compartments with discrete separation from flanking DNA regions. Little specific organization was scored within these domains, suggesting mostly random contacts. Furthermore, these association domains precisely matched the distribution of H3K27me3 marks decorating these loci (Fig. 1C and figs. S7 to S9), both in the positions of the borders and in the organization within each cluster, supporting a functional interplay between these two parameters in vivo (*10*).

We examined these architectures in "anterior" and "posterior" embryonic tissue samples, where different *HoxD* genes are transcribed at this stage of development (Fig. 2 and fig. S10). In contrast to the single interaction domain observed in brain cells (Fig. 2, A to C, green), both anterior (in red) and posterior (in blue) trunk cells generated bimodal profiles of association, dividing the gene cluster into two distinct 3D compartments. However, the boundaries between these two compartments were located at different positions in anterior versus posterior trunk samples. In anterior trunk, transcribed genes like *Hoxd4* no longer contacted the silent (centromeric) part of the cluster, thus forming an "active domain" (Fig. 2A). Accordingly, *Hoxd13*, the most centromeric gene, no longer contacted the telomeric part of the cluster (Fig. 2C, "inactive domain"). The transition of genes from an inactive to an active 3D domain was best exemplified by *Hoxd9*, expressed strongly in posterior trunk cells but only weakly in the anterior sample (Fig. 2B and fig. S1). Contacts of *Hoxd9* were stronger with the centromeric part of the cluster in anterior cells (gene mostly off; in the "inactive domain"), but they clearly shifted toward the telomeric part of the cluster in posterior trunk cells (gene on, "active domain"; Fig. 2B, see ratio). The same was observed for *Hoxd11*, which strongly contacted the negative domain in anterior trunk cells (off state), whereas most contacts were with the positive domain in posterior trunk cells (on state; fig. S10). This bimodal organization also applied to the other three

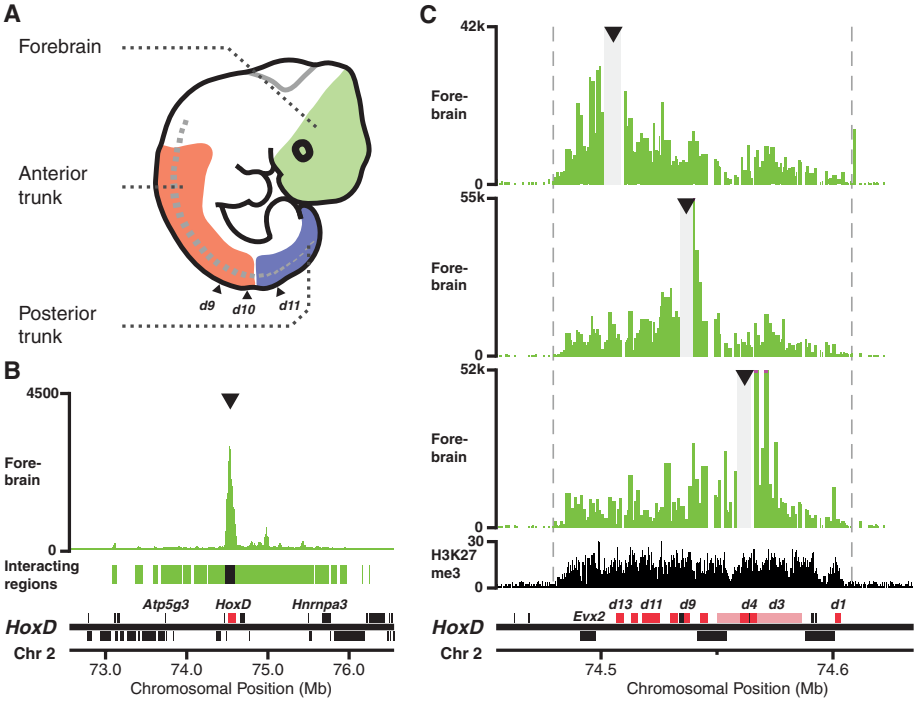

Fig. 1. The inactive *HoxD* cluster forms a discrete 3D compartment. (**A**) Schematized E10.5 mouse embryo highlighting tissue samples used in this work: forebrain (green), anterior trunk (red), and posterior trunk (blue). Approximate positions of expression boundaries for either *Hoxd9* (d9), *Hoxd10* (d10), or *Hoxd11* (d11) are indicated with arrowheads. (**B**) Running-mean 4C-seq interaction patterns of *Hoxd9* in a 4-Mb-large genomic region surrounding the *HoxD* cluster in forebrain tissue. Significant interactions are depicted below (see also fig. S6). The position of the *HoxD* cluster is shown in red, flanked by two gene deserts (below). (**C**) Quantitative local 4C-seq interactions reveal the local 3D domain of the inactive *HoxD* cluster (forebrain). Below, H3K27me3 signal is aligned. Dashed lines emphasize the discrete borders of the local 3D domain and the coincidence with the H3K27me3 domain. Three viewpoints are used (*Hoxd13*, *Hoxd9*, and *Hoxd4*, from top to bottom) and are indicated with arrowheads. Excluded regions around these viewpoints are depicted with vertical light gray boxes. The locations of *Hoxd* genes (red) and of other transcripts (black) are shown below.

[1]National Research Centre "Frontiers in Genetics," School of Life Sciences, Ecole Polytechnique Fédérale (EPFL), Lausanne, CH-1015, Switzerland. [2]Hubrecht Institute and University Medical Center, Utrecht, 3584 CT, Netherlands. [3]Swiss Institute of Bioinformatics, Lausanne, CH-1015, Switzerland. [4]Department of Genetics and Evolution, University of Geneva, CH-1211, Switzerland.

*To whom correspondence should be addressed. E-mail: denis.duboule@unige.ch or denis.duboule@epfl.ch

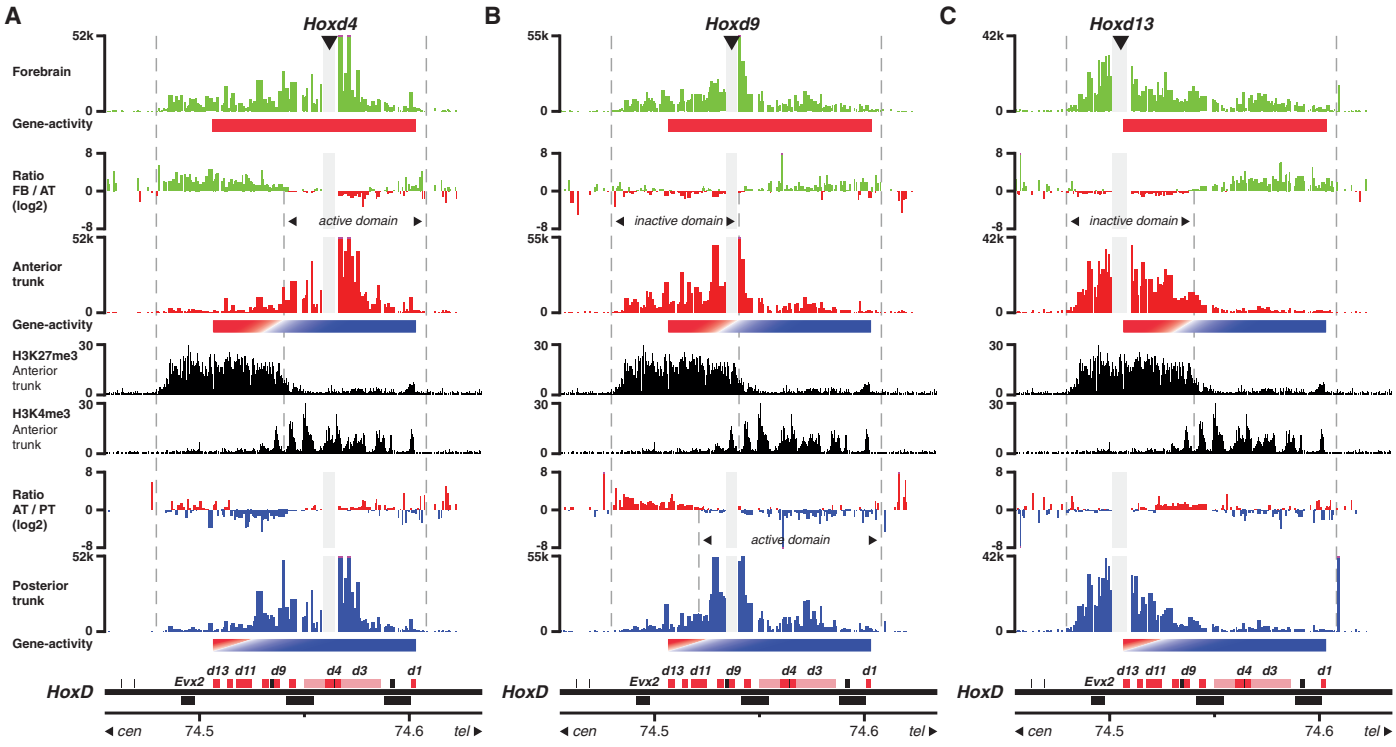

Fig. 2. Dynamic architectures of the *HoxD* cluster at different stages of colinear activation. The frequencies of associations are shown with *Hoxd4* (**A**), *Hoxd9* (**B**), or *Hoxd13* (**C**) as viewpoints in forebrain (profiles in green), anterior trunk (profiles in red), or posterior trunk (profiles in blue) tissues. The ratios of interactions are indicated between the profiles for the same viewpoint in different embryonic tissues. The colinear expression status (blue, active; red, inactive) of *Hoxd* genes (bottom line) is schematized below each profile. For the anterior trunk sample (in red), the corresponding H3K27me3 and H3K4me3 signals are indicated just below (profiles in black). Residence of viewpoints in the active [(A), anterior trunk *Hoxd4* and (B), posterior trunk *Hoxd9*] and inactive [(B), anterior trunk *Hoxd9* and (C), anterior trunk *Hoxd13*] domains is indicated with arrowheads.

Hox clusters, with slight variations in the location of the internal boundary, depending on the progression of gene activation within each cluster (fig. S11).

In the trunk samples, not only did we observe a coincidence between the inactive 3D domain and the extent of H3K27me3 modifications, as in the brain sample, but the active compartments also matched the presence of H3K4me3 chromatin domains (Fig. 2, A to C, and figs. S9 to S11). The distribution of these chromatin marks correlated with the 3D organization at these *Hox* clusters. In this context, the *HoxB* cluster was particularly interesting because an 80-kb, repeat-rich intergenic region separates *Hoxb13* from the rest of the cluster (*14*). Using viewpoints in the cluster and within this intergenic region, we observed a weak association only (if any) between this region and the rest of the *HoxB* cluster (fig. S12), suggesting that it loops out from this bimodal architecture. The same interruption was seen in the distribution of H3K27me3 marks (fig. S12), illustrating again the precise correspondence between chromatin marks and 3D architecture and showing that these spatial domains do not necessarily involve an uninterrupted linear chromatin fiber. This latter conclusion was further illustrated by strongly increased and targeted associations between the inactive domain of the *HoxD* cluster (*Hoxd13*) and the *Dlx1* locus, which are separated by a distance of 3 Mb and both heavily decorated with H3K27me3 marks (fig. S13). In contrast, such interactions were not scored with the active part of the *HoxD* cluster.

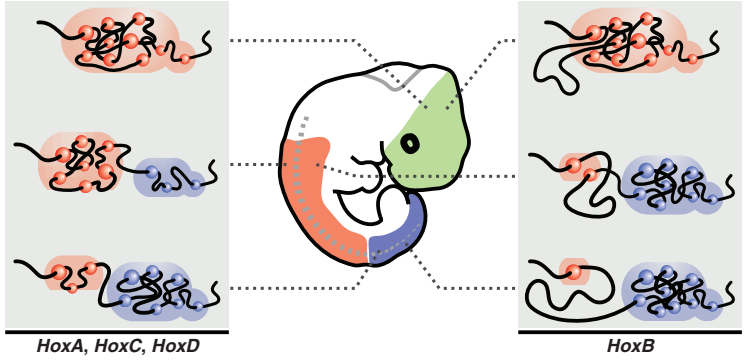

Fig. 3. Model of the 3D organization of *Hox* gene clusters, at various stages of colinear gene activation. Transcriptionally inactive genes are depicted in red and active genes in blue. Gene activation is paralleled by a transition from one 3D domain, matching the presence of H3K27me3, to another domain of active transcription (marked with H3K4me3). Although the same dynamics are observed for the *HoxA*, *HoxC*, and *HoxD* clusters (left), the *HoxB* cluster (right) shows a slight variation with a large piece of intergenic DNA looping out from these two domains.

From these data sets, we propose a model whereby *Hox* genes move stepwise from an inactive compartment marked by H3K27me3 to another, transcriptionally active domain labeled with H3K4me3 marks (Fig. 3). We challenged this view by using two deletions in vivo where *Hox* gene activities are differentially perturbed (*15*). Deletion of the *Hoxd8* to *Hoxd10* DNA fragment [Del(*8–10*)] does not severely change the expression of *Hoxd11* (fig. S14). However, the additional deletion of the intergenic region *i* [Del(*i8-10*)] results in a strong activation of *Hoxd11* in anterior tissues (fig. S14). These overlapping deletions thus have distinct transcriptional outcomes, with *Hoxd11* ectopically activated in the anterior trunk sample of Del(*i8-10*) embryos

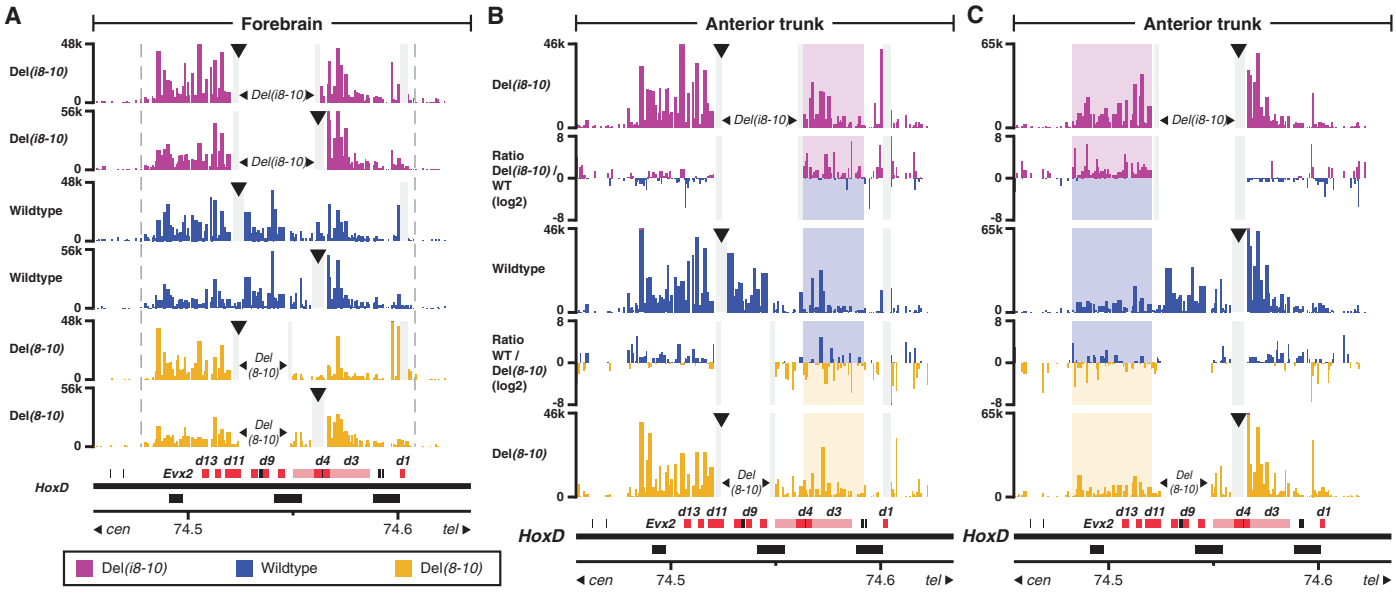

Fig. 4. Ectopic activation of *Hoxd11* in anterior tissue increases its association frequency with other active *Hoxd* genes. (**A**) Three-dimensional organization of the inactive *HoxD* cluster in wild-type forebrain (blue profiles, middle) or in forebrain tissues carrying two distinct internal deletions into the *HoxD* cluster [Del(*i8-10*), profiles in purple on the top, and Del(*8-10*), profiles in yellow, bottom]. The deletions are indicated between small arrowheads and, for each sample, both *Hoxd11* and *Hoxd4* are used as viewpoints (large arrowheads). Regardless of cluster size, the 3D inactive domains remain demarcated by the same outside borders. (**B**) Three-dimensional organization of mutant *HoxD* clusters in anterior trunk with *Hoxd11* as a viewpoint (arrowhead). *Hoxd11* is expressed ectopically in the Del(*i8-10*) mutant anterior tissue, but not in the Del(*8-10*) mutant (see figs. S14 to S17). Accordingly, increased association frequencies are observed between *Hoxd11* and the active part of the cluster in the Del(*i8-10*) mutant (purple box and ratio), as compared to both wild-type (in blue) and the Del(*8–10*) mutant embryos (yellow box and ratio). (**C**) Same experiment as in (B), but with *Hoxd4* as a viewpoint (arrowhead). Again, interactions are increased between *Hoxd4* and the posterior part of the *HoxD* cluster (purple box and ratio) containing *Hoxd11*, which is ectopically expressed in the mutant Del(*i8-10*) anterior tissue. In contrast, the Del(*8-10*) mutant tissue, where *Hoxd11* is not expressed anteriorly, does not show such increased interactions (yellow box and ratio).

only. We first assessed whether such deletions had changed the overall cluster architecture in brain cells (Fig. 4A and figs. S15 and S16) and observed that the inactive domains maintained the same borders on both sides, indicating that the mechanism underlying this 3D compartmentalization is likely intrinsic to the gene cluster. We then studied the interaction profiles using *Hoxd11* and *Hoxd4* as viewpoints in anterior trunk samples (Fig. 4, B and C, and fig. S17). In the Del(*i8-10*) mutant, where *Hoxd11* is ectopically activated (*15*), the association between *Hoxd11* and the "positive" compartment was strongly increased. This was scored either by using *Hoxd11* as a viewpoint (Fig. 4B, shaded purple/blue ratio), or *Hoxd4* (Fig. 4C, shaded purple/blue ratio). However, contacts remained as in wild-type embryos when the shorter Del(*8–10*) deletion was analyzed with the same viewpoints (Fig. 4, B and C, shaded blue/yellow ratios). Ectopic activation, rather than a deletion per se, was thus paralleled by enhanced association between *Hoxd11* and the "active" anterior domain.

This work suggests that the colinear activation of *Hox* genes involves a stepwise transition of each gene from a negative to a positive compartment, which display different biochemical properties and thus results in a physical separation of their regulatory modalities. Although it remains to be fully demonstrated whether such a process underlies colinear activation or is a consequence of it, it is noteworthy that the former possibility would provide a mechanistic solution to three crucial problems encountered during the activation of this gene family: (i) to ensure a proper colinear sequence in gene activation, such that axial morphologies are respected [see e.g., (*16*)]; (ii) to prevent the most posterior genes from being activated too early, which leads to deleterious phenotypes (*17*); and (iii) to fix and memorize transcriptional states at various body levels. These critical constraints are well addressed by our cis-acting model, whereas other potential mechanisms, such as relying upon trans-acting interactions, may not allow the same level of precision and reliability.

References and Notes

1. M. Kmita, D. Duboule, *Science* **301**, 331 (2003).
2. R. Krumlauf, *Cell* **78**, 191 (1994).
3. N. Soshnikova, D. Duboule, *Science* **324**, 1320 (2009).
4. R. J. Palstra *et al.*, *Nat. Genet.* **35**, 190 (2003).
5. M. A. Ferraiuolo *et al.*, *Nucleic Acids Res.* **38**, 7472 (2010).
6. J. Fraser *et al.*, *Genome Biol.* **10**, R37 (2009).
7. K. C. Wang *et al.*, *Nature* **472**, 120 (2011).
8. S. Chambeyron, W. A. Bickmore, *Genes Dev.* **18**, 1119 (2004).
9. C. Morey, N. R. Da Silva, M. Kmita, D. Duboule, W. A. Bickmore, *J. Cell Sci.* **121**, 571 (2008).
10. R. Eskeland *et al.*, *Mol. Cell* **38**, 452 (2010).
11. Material and methods are available as supporting material on *Science* Online.
12. M. Simonis *et al.*, *Nat. Genet.* **38**, 1348 (2006).
13. A. P. Lee, E. G. Koh, A. Tay, S. Brenner, B. Venkatesh, *Proc. Natl. Acad. Sci. U.S.A.* **103**, 6994 (2006).
14. L. Zeltser, C. Desplan, N. Heintz, *Development* **122**, 2475 (1996).
15. P. Tschopp, B. Tarchini, F. Spitz, J. Zakany, D. Duboule, *PLoS Genet.* **5**, e1000398 (2009).
16. D. M. Wellik, *Dev. Dyn.* **236**, 2454 (2007).
17. T. Young *et al.*, *Dev. Cell* **17**, 516 (2009).

Acknowledgments: We thank B. Mascrez for assistance with mouse handling and genotyping, P. Descombes and members of the National Research Centre genomics platform for high-throughput sequencing, and members of the Duboule laboratories for discussion. Computations were performed at the Vital-IT Center for high-performance computing (www.vital-it.ch) at the Swiss Institute of Bioinformatics. This work was supported by funds from the Ecole Polytechnique Fédérale (Lausanne), the University of Geneva, the Swiss National Research Fund, the National Research Centre "Frontiers in Genetics," and the European Research Council grant SystemsHox.ch (to D.D.). Data are all based on ENSEMBL Mouse assembly NCBIM37. 4C-seq patterns can be obtained from www.sciencemag.org/nnnnn or http://duboule-lab.epfl.ch/page-66605-en.html. Microarray and ChIP-seq data have been submitted to the Gene Expression Omnibus (GEO) repository (www.ncbi.nlm.nih.gov/geo/) under accession no. GSE31570.

Supporting Online Material

www.sciencemag.org/cgi/content/full/334/6053/222/DC1
Materials and Methods
Figs. S1 to S17
Tables S1 to S6
References (*18–24*)

19 April 2011; accepted 17 August 2011
10.1126/science.1207194